sustainability

MDPI

Article

Chemical Modification of Combusted Coal Gangue for U(VI) Adsorption: Towards a Waste Control by Waste Strategy

Yuan Gao [1,†], Jiandong Huang [2,†], Meng Li [2], Zhongran Dai [3], Rongli Jiang [1] and Jixiong Zhang [2,*]

[1] School of Chemical Engineering and Technology, China University of Mining & Technology, Xuzhou 221116, China; y.gao@cumt.edu.cn (Y.G.); ronglijcumt@163.com (R.J.)
[2] School of Mines, China University of Mining & Technology, Xuzhou 221116, China; huang@cumt.edu.cn (J.H.); limeng77521@126.com (M.L.)
[3] Key Discipline Laboratory for National Defense for Biotechnology in Uranium Mining and Hydrometallurgy, University of South China, Hengyang 421001, China; dzr1122@126.com
* Correspondence: cumtzjxiong@163.com
† Yuan Gao and Jiandong Huang have equal contribution to this work.

Abstract: Uranium mining waste causes serious radiation-related health and environmental problems. This has encouraged efforts toward U(VI) removal with low cost and high efficiency. Typical uranium adsorbents, such as polymers, geopolymers, zeolites, and MOFs, and their associated high costs limit their practical applications. In this regard, this work found that the natural combusted coal gangue (CCG) could be a potential precursor of cheap sorbents to eliminate U(VI). The removal efficiency was modulated by chemical activation under acid and alkaline conditions, obtaining HCG (CCG activated with HCl) and KCG (CCG activated with KOH), respectively. The detailed structural analysis uncovered that those natural mineral substances, including quartz and kaolinite, were the main components in CCG and HCG. One of the key findings was that kalsilite formed in KCG under a mild synthetic condition can conspicuous enhance the affinity towards U(VI). The best equilibrium adsorption capacity with KCG was observed to be 140 mg/g under pH 6 within 120 min, following a pseudo-second-order kinetic model. To understand the improved adsorption performance, an adsorption mechanism was proposed by evaluating the pH of uranyl solutions, adsorbent dosage, as well as contact time. Combining with the structural analysis, this revealed that the uranyl adsorption process was mainly governed by chemisorption. This study gave rise to a utilization approach for CCG to obtain cost-effective adsorbents and paved a novel way towards eliminating uranium by a waste control by waste strategy.

Keywords: combusted coal gangue; chemical modification; uranium; adsorption

Citation: Gao, Y.; Huang, J.; Li, M.; Dai, Z.; Jiang, R.; Zhang, J. Chemical Modification of Combusted Coal Gangue for U(VI) Adsorption: Towards a Waste Control by Waste Strategy. *Sustainability* **2021**, *13*, 8421. https://doi.org/10.3390/su13158421

Academic Editor: Avelino Núñez-Delgado

Received: 5 July 2021
Accepted: 24 July 2021
Published: 28 July 2021

1. Introduction

Even with the growth of renewables and natural gas, coal resources are still the primary fuel to provide energy for daily life and industry. However, coal mining activities lead to various wastes, including CO_2 emissions [1,2], heavy metal-induced acid mine drainage [3], and coal gangue heap [4]. Among them, the accumulation of coal gangue (CG) and combusted coal gangue (CCG) without appropriate utilization has resulted in land occupation, landscape destruction, as well as heavy metal pollutions [5]. Currently, coal gangue is mainly used in the field of backfilling, building materials, agriculture, energy generation, soil improvement, and other high-added applications [6–8].

Nuclear power can partially substitute fossil energy and provide low-cost electrical power [9]. However, uranium used in the nuclear reactor is radiative, which causes both environmental and health issues [10]. Considering the rapid growth in uranium demand, efficient methods are necessary to eliminate or reduce uranium from contaminated media. Numerous methods, such as ion exchange, chemical precipitation, chromatographic extraction, and electrochemical techniques, have been developed to deal with uranium

contaminations [11]. Among them, adsorptions show the most promising method due to their easy-handling and efficiency [12,13]. The designed synthesized materials, such as polymers, geopolymers, zeolites, and MOFs, have been applied in the removal of U(VI) [14]. These materials feature high surface area, uniform pore structure, excellent stability, and thus high sorption capacities [15]. The functional species, such as the hydroxyl, phosphoryl oxygen and metal oxide, were found to have strong interactions with U(VI). However, the associated high cost of precursors limits their practical applications.

In general, the CG and CCG contain natural mineral adsorbents, such as quartz, kaolinite, illite, chlorite, feldspar, and calcite. Due to the huge production and low-cost, the adsorption on constituents of CG and CCG was tested in environmental related remediation in the early stage. The main challenge of using them as a commercial adsorbents is due to a low surface area, pores, low ion exchange, and as a result low adsorption capacity [16]. Recently, chemical activations by mixing CG and CCG with strong alkali (e.g., Na_2SiO_3, NaOH and KOH) or and acidic solutions (e.g., HCl) has been investigated, which can open the pores increase the surface area of particles through disaggregation, elimination of mineral impurities, and dissolution of the external layers. An alkali solution dissolves aluminosilicate-reactive materials and forms AlO_4 and SiO_4 tetrahedral units that polysialate disiloxo (Al-O-Si-Si-Si chain), Al-O-Si chain, and siloxo Al-O-Si-Si-Si chain. Some studies also believe that instead of forming polymers, SiO_4^{4-} and AlO_4^{5-} can be dissolved by breaking the skeleton of aluminosilicate, depending on the alkali type and concentrations [17,18]. Using modified CG as promising adsorbents has been performed on adsorptions of methylene blue and heavy metal ions, including Cu^{2+}, Cd^{2+} Zn^{2+}, and Pb^{2+} [19,20].

Despite the studies mentioned above, a systematic analysis of the chemical activation of CG and CCG, with a wide characterization of the obtained solids and a complete discussion of their structural differences, is lacking in the literature. The increasing interest in adsorption applications of natural, quite common, and cheap materials justifies such a systematic study of this process [19–25]. Regarding that radioactivity U(VI) and coal gangue are coexistent wastes in certain cases, the target of this work is not only to eliminate them by a low-cost strategy, but also to deeply understand the active adsorption component, under chemical treatments, of CCG [26,27]. Herein, we report the results of uranyl adsorption under various experimental conditions using a CCG-based adsorbents, HCG and KCG. The roles played by surface properties and constitutions were explained based on characterizations and mechanistic studies.

2. Results and Discussion

2.1. Characterizations

The details of the synthetic approach are described in the Supplementary Materials and illustrated in Scheme 1. To confirm the successful chemical-modification of CCG, detailed characterizations of all the materials were performed by FTIR, PXRD, TGA-DSC, XPS, and SEM measurements. As shown in Figure 1 (left), the PXRD patterns of the solids treated with acid at room temperature did not show significant variations with respect to quartz and kaolinite, which are the major mineralogical composition of CCG and HCG. The acid treatment produced the dissolution of Ca^{2+}, Mg^{2+} cations, provoking a relatively increased crystallinity in the HCG constitutions due to the increased purity and concentrations of quartz and kaolinite. In contrast, treatment with KOH at room temperature led to weak alternations in the composition and structure of the solids. The first strong difference observed in PXRD is that the characteristic patterns of kaolinite phase decreased and the patterns with new peaks were observed. The comparison of the new diffractograms with the PDF data file shows that the feldspathoid kalsilite ($KAlSiO_4$) was formed under this reaction condition, which has a framework of linked (Si, Al)O_4 tetrahedra, and corresponding PXRD peaks are located at 19°, 21°, and 28° [28–30].

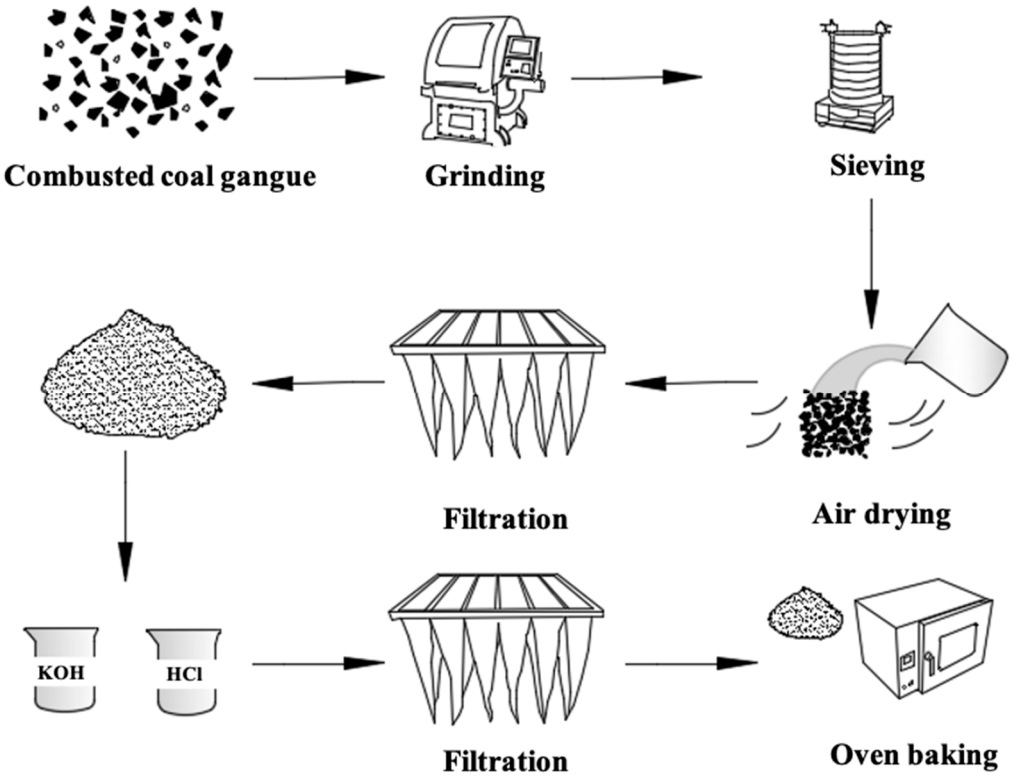

Scheme 1. The modification approach of CCG.

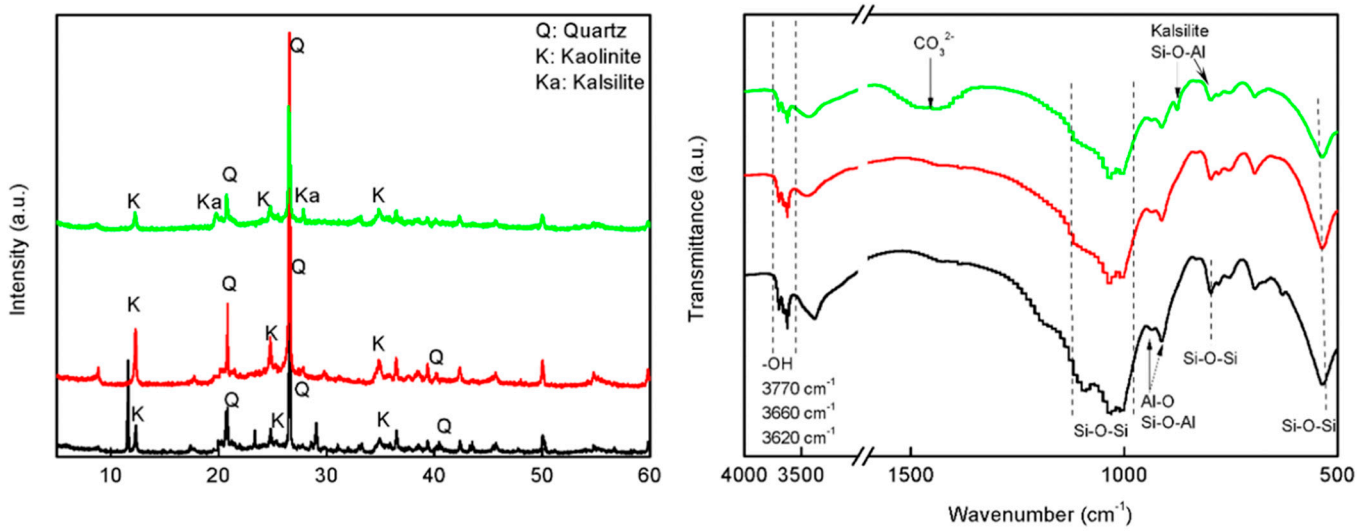

Figure 1. The PXRD (**left**) and FTIR (**right**) of CCG (black), HCG (red) and KCG (green).

FTIR spectrum showed the typical bands of quartz and kaolinite in CCG and HCG (Figure 1 (right)). Thus, the bands assigned to O-H stretching vibration in kaolinite were found at 3700, 3660, and 3620 cm^{-1} [31]. Meanwhile, the Al-O and Si-O-Al vibration from kaolinite can be found at 915 and 900 cm^{-1}. In this region of low wavenumbers, there are characteristic peaks of quartz: 1098, 1035, 1010, and 781cm^{-1} (Si-O-Si vibration). FTIR spectra of CCG treated with KOH showed the characteristic patterns of kalsilite, where the appearance of 987 cm^{-1} and 689 cm^{-1} peak assigned to Si-O-Al asymmetric stretching vibration in the linked (Si, Al)O_4 tetrahedra [32].

To further characterize the surface property of the prepared samples, the binding energies of C1s, O1s, Al2p, and Si2p as well as trace elements were determined by XPS

(Supplementary Figure S1), a magnified view of which is shown in Figure 2. There were no significant differences in the binding energy of Al2p, Si2p in CCG and HCG, while these peaks shifted to lower binding energy in KCG. Distinct variation in peak area also revealed changes in chemical structure [33]. As compared with CCG (1/1.40) and HCG (1/1.46), the increased ratio of Al/Si (1/1.26) in KCG was caused by the minor kalsilite formation. This suggests the alkaline treatment promoted an aluminum enrichment surface, while acid modification is on the contrary. These results are consistent with reported studies [34]. Moreover, the aluminum on the surface is always regarded as the active site compared to Si, which can influence adsorption as well as related physical properties [33].

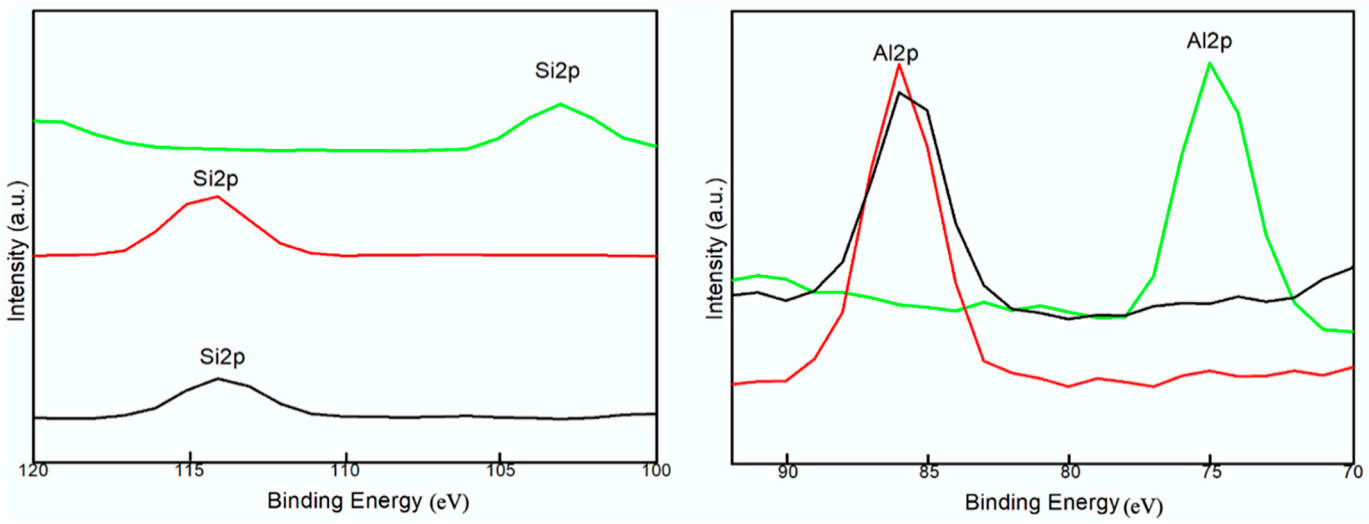

Figure 2. The zoom in XPS analysis of Si2p and Al2p in CCG (black), HCG (red) and KCG (green).

The thermogravimetric analysis showed that higher decomposition temperature was observed in all samples between 450 and 500 °C, whilst the KCG exhibited a dramatical weight loss below 200 °C as compared with CCG and HCG (Supplementary Figure S2). This can be related to the evaporation of lattice water, and explained by a larger pores and relatively high surface area in the KCG sample [31,34]. The accurate surface area and pore distributions of CCG, HCG, and KCG were investigated by nitrogen adsorption-desorption measurements, and the results are shown in Supplementary Figure S3. The CCG already showed certain porosity and activity, with a surface area of 21.34 m^2/g and a pore volume of 0.03 cm^3/g. This is larger than the reported mechanical activation coal gangue [34]. After chemical modifications, the BET surface area and a pore volume of samples increased conspicuously as compared to CCG (Table 1). Combined with the above characterizations, the increased surface in the HCG can be explained by the dissolution of metal ions. The improved surface property of KCG could be attributed to kalsilite formation.

Table 1. The calculation of BET surface area, pore volume and pore size by the Barrett-Joyner-Halenda analysis.

Sample	BET Surface Area (m^2/g)	Pore Volume (cm^3/g)	Pore Size (nm)	Standard Deviation of Fit (cm^3/g)
CCG	21.34	0.03	7.43	0.112
HCG	44.7	0.063	5.36	0.340
KCG	62.33	0.088	5.98	0.450

The surface features also related to the morphology of particles, therefore we conducted SEM measurements (Figure 3). Briefly, the structure of as-synthesized HCG and KCG became relatively loose after chemical modification. The surface of fresh CCG was relatively dense, and there were no large pores or fractures. The activated HCG and KCG

presented decreased particle size and some irregular layered structures, which contribute to increased surface areas.

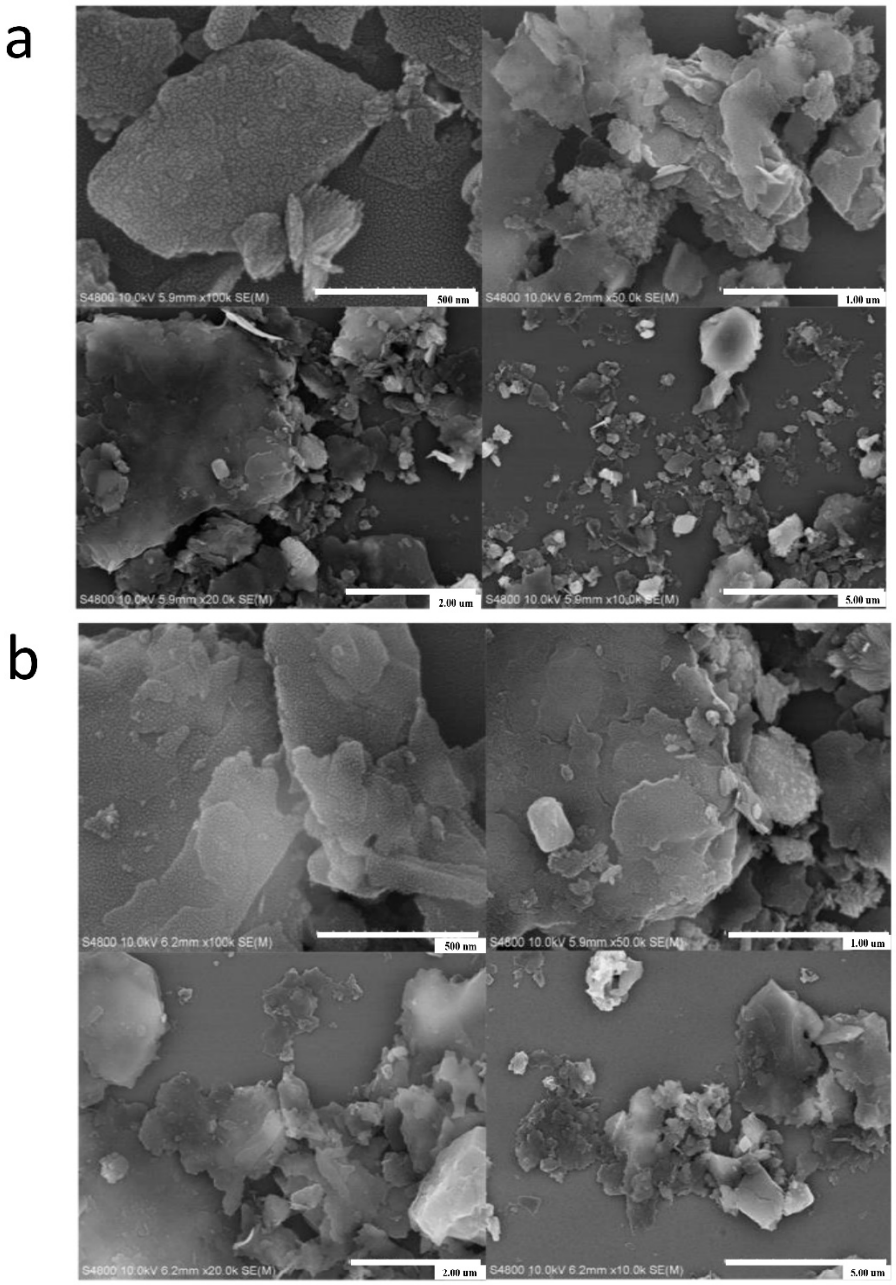

Figure 3. *Cont*.

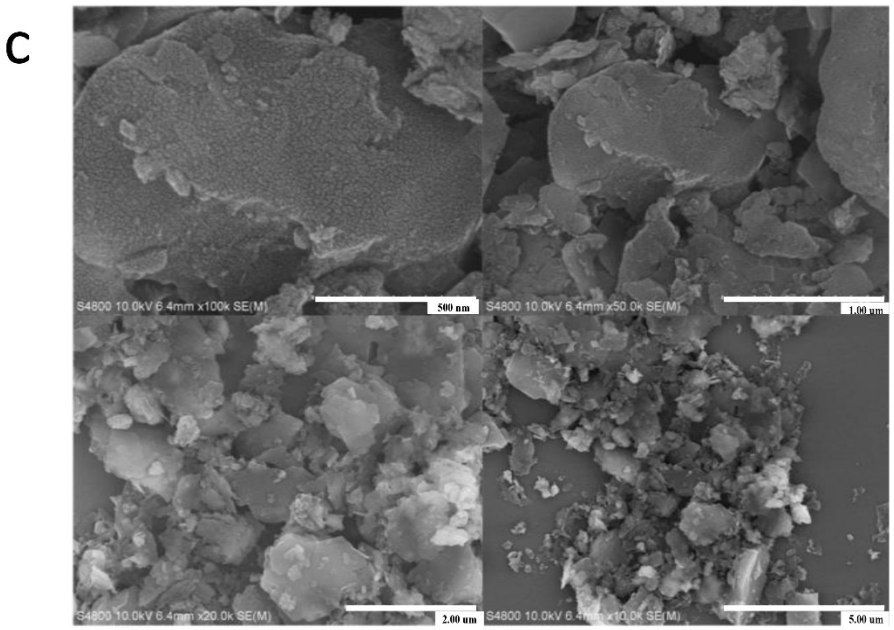

Figure 3. The SEM images of CCG (**a**), HCG (**b**) and KCG (**c**) at 500 nm, 1.00 um, 2.00 um, and 5.00 um.

2.2. Adsorption Performance

The above characterizations, including crystallinity, functional groups, surface area, and pore volume, are key factors affecting adsorption process. Based on these, the batch experiments were carried out to investigate the UO_2^{2+} adsorption on CCG, HCG, and KCG samples.

2.2.1. Effect of pH

The acidity not only determines the existing forms of the targets, but influences the surface charge of the adsorbents, due to the repulsion forces and electrostatic attractions occurring between adsorbents and the U(VI) ions [35,36]. The U(VI) is in the style of cationic with a positive charge in solution. Thus, the surface charge of the modified coal gangue is strongly influenced by the pH of the solution. It can be noticed that uranyl carbonate starts to form from pH 6.5 as the predominant species, and the negative charge of uranyl carbonate will compromise the adsorption on the coal gangue surface. Therefore, we selected the batch experiments conducted from pH 2 to 6.

As depicted in Figure 4, CCG showed the removal efficiency from 2.1% to 15.2% under the pH from 2 to 6. The corresponding adsorption capacity increased from 4.2 to 39.6 mg/g. Generally, a more acidic solution can induce the protonation of reactive sites. For the kaolinite and quartz, the number of negatively charged sites, including Al-O^- and Si-O^-, increases under an increase in pH conditions [37,38]. As a result, the electrostatic attractions between the positive U(VI) and negative adsorbents became stronger and the removal percentage increased. These pH effects can explain the increasing adsorption trends of all samples (Figure 4 and Supplementary Table S1). Although HCG and KCG have improved porosity and surface area, the removal percentage of uranium by HCG slightly increased to 14.6% (43.8 mg/g) at pH 6. Meanwhile, KCG reflected a much higher adsorption performance than that of HCG, reaching the adsorption capacity of 140 mg/g. The improved adsorption properties can be explained by the fact that Al of lower binding energy has a higher affinity towards U(VI), and therefore KCG with a higher Al/Si (1/1.26) ratio leads to a better adsorption performance [39].

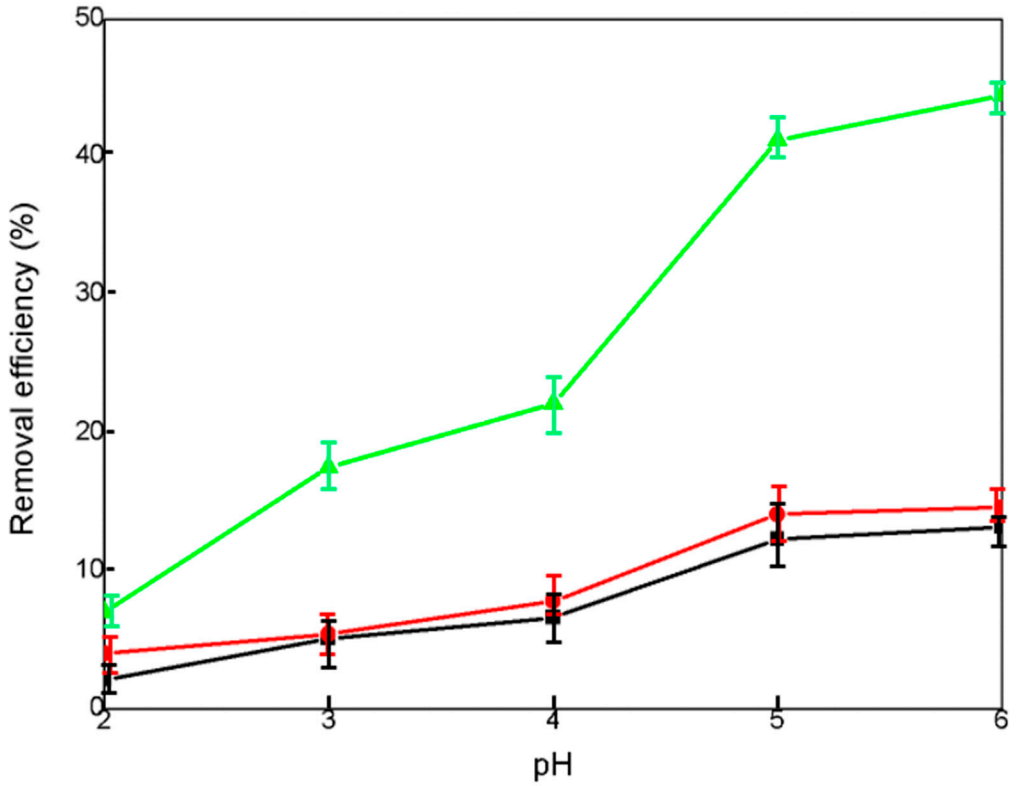

Figure 4. Removal efficiency (%) with 5 mg CCG (black), HCG (red) and KCG (green) adsorbents in 30 mL U(VI) (50 mg·L^{-1}) solution under variant pH conditions (from 2 to 6).

2.2.2. Effect of Adsorbent Dosage

Generally, the adsorption capacity of metal ions is determined by the amount of available adsorption sites on the adsorbents depends on the size and free energy of the hydrated ions, the activity of the metal ions, and other intrinsic reasons. As adsorbent dosage increases keeping all the other parameters at constant value, the removal efficiency of HCG increased continuously. The KCG sample, however, showed first increases, reached maximum and then decreased to zero, due to the precipitation of uranium by basic sites (Figure 5).

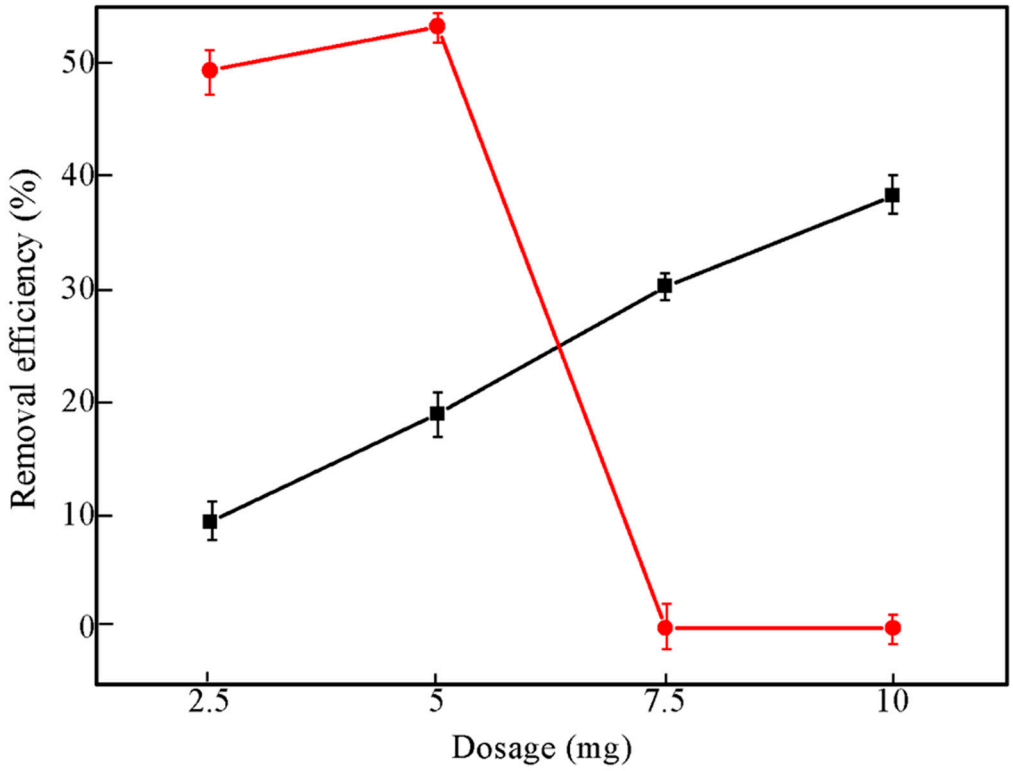

Figure 5. The effect of adsorbent dosage of HCG (black), and KCG (red) that influence the U(VI) adsorption.

2.2.3. Influence of Contact Time and Adsorption Kinetics

Supplementary Figure S4 shows the UO_2^{2+} evolution with the contact time. The removal efficiency of U(VI) adsorption onto HCG reached to 15% within 120 min, and then increased slightly with contact time and reached 15.6% at 120 min. The high removal efficiency of KCG reached equilibrium 41% within 120 min. To evaluate the adsorption rates of uranium ions onto HCG and KCG, the kinetics experiments were fitted by pseudo first-order and pseudo second-order kinetic models. The specific kinetic parameters as well as the calculated adsorption rates are shown in Table 2.

Table 2. Parameters of the pseudo-first-order and pseudo-second-order kinetic models for adsorption of U(VI) on HCG and KCG under pH 6.

Adsorbents	Pseudo-First-Order			Pseudo-Second-Order		
	R^2	q_e (mg/g)	K_1 (g/mg/min)	R^2	q_e (mg/g)	K_2 (g/mg/min)
HCG	0.985	22.8	−0.03	0.999	47.6	0.00412
KCG	0.955	126.8	−0.038	0.999	144.9	0.000667

As depicted in Figure 6, the pseudo second-order model provided a relatively high correlation coefficient (R^2 = 0.999). Moreover, the calculated q_e values of 47.6 mg/g and 145 mg/g from second-order was closed to the experimental data (46.8 mg/g and 140 mg/g, respectively), which suggested that the UO_2^{2+} ion adsorption onto HCG and KCG was mainly governed by chemisorption, which included diffusion, adsorption, and interior pore diffusion. The two-step immobilization process was assumed in chemical adsorption: (i) UO_2^{2+} moved to the surface of the HCG and KCG; (ii) UO_2^{2+} ions diverted from their surface to the active sites on the interior pore.

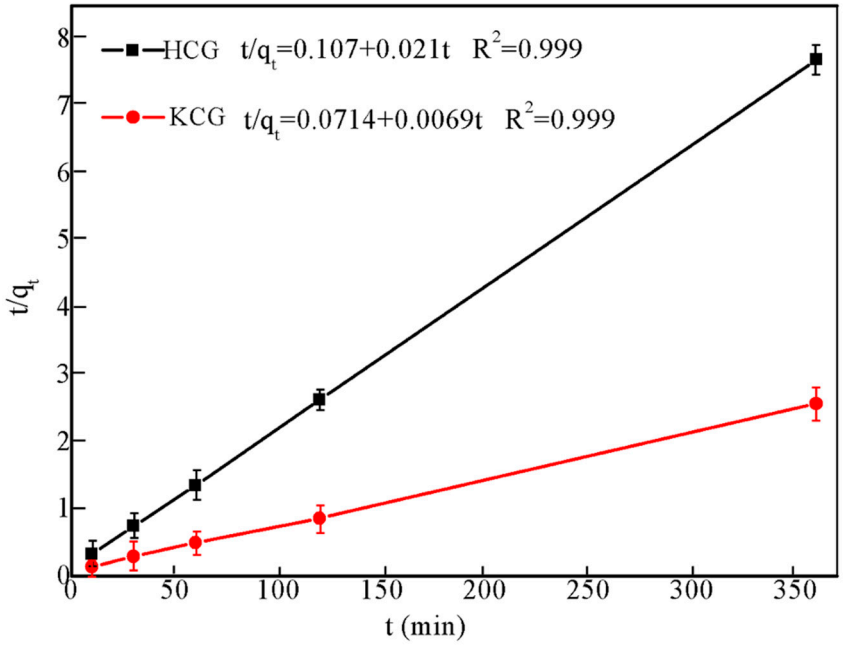

Figure 6. Adsorption kinetics of U(VI) on HCG (black) and KCG (red) fitted to pseudo-second-order kinetic model under pH 6.

2.2.4. Adsorption Mechanism

The structural characterizations and batch adsorption experiments showed that the structure optimization improved the adsorption properties of KCG controlled by chemical adsorption. In order to clarify the nature of the interaction of uranyl with adsorbents, the structure changes after adsorption were measured and analyzed by FTIR, PXRD, SEM, and XPS.

The comparison FTIR spectra before and after adsorption are shown in Figure 7 (left). The Al-O, Si-O, and Al-O-Si from kaolinite and kalsilite played an important role in the creation chemical bonding between adsorbents and U(VI), due to the disappear and/or shift of these bands together with the observation of SiO-UO_2^{2+}, AlO-UO_2^{2+}, and UO_2^{2+}-Si-O-Al-UO_2^{2+} [40]. The kalsilite formed in KCG had strong interactions with U(VI), and thus prominently improved the adsorption capacity, which can be confirmed by PXRD.

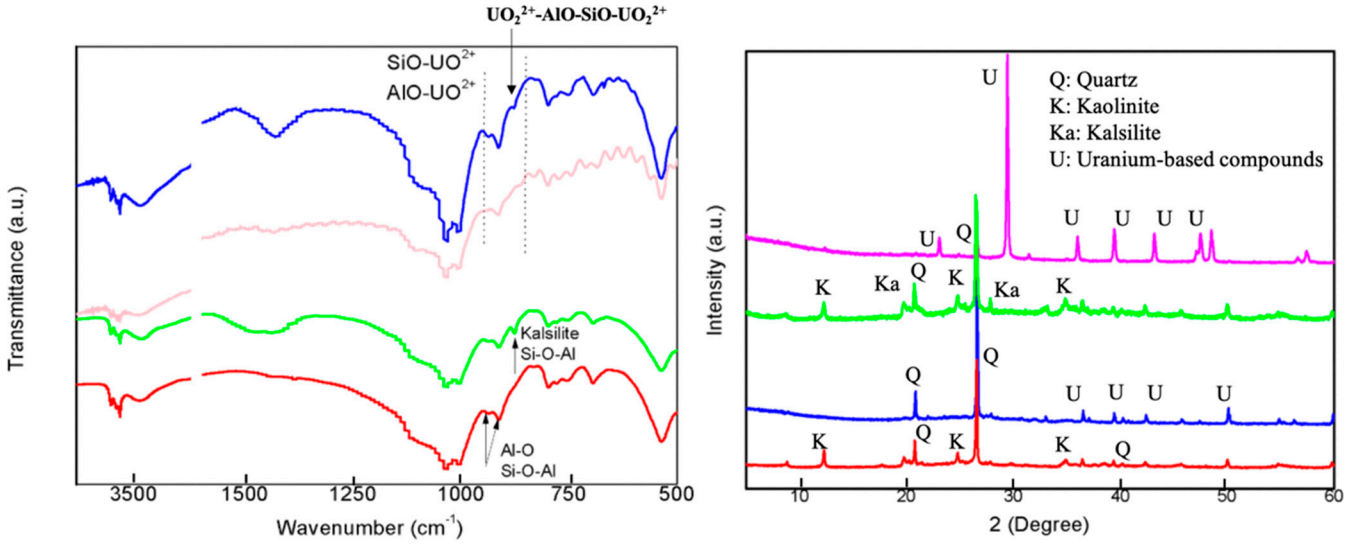

Figure 7. The FTIR (**left**) and PXRD (**right**) before and after UO_2^{2+} adsorption of HCG (red) and after adsorption (blue), KCG (green) and after adsorption (pink).

In Figure 7 (right), the crystalline phases in HCG are retained, while obvious changes can be observed in KCG after uranium adsorption, indicating the creation of new chemical bonding. XPS showed obvious U4f peaks at 382 eV in Figure 8 (left). Especially the atomic percentage of Si2s, Si2p, Al2s, and Al2p in KCG had a sharp decrease due to the higher loading of U(VI). Indeed, additional confirmation of chemical adsorption came from SEM, which displayed that the surface of adsorbents before uranium adsorption is smooth, but became rough and irregularly shaped after uranium adsorption (Figure 9). All these results show that the improved adsorption property is controlled by strong chemical interactions in KCG.

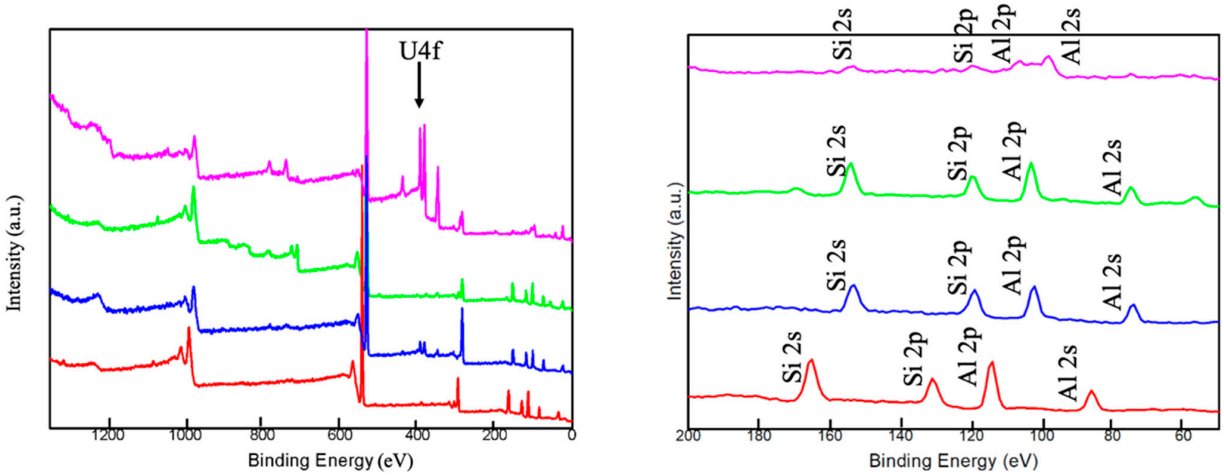

Figure 8. The XPS analysis before and after UO_2^{2+} adsorption of HCG (red) and after adsorption (blue), KCG (green) and after adsorption (pink). The right is the zoom in the analysis of Si and Al elements.

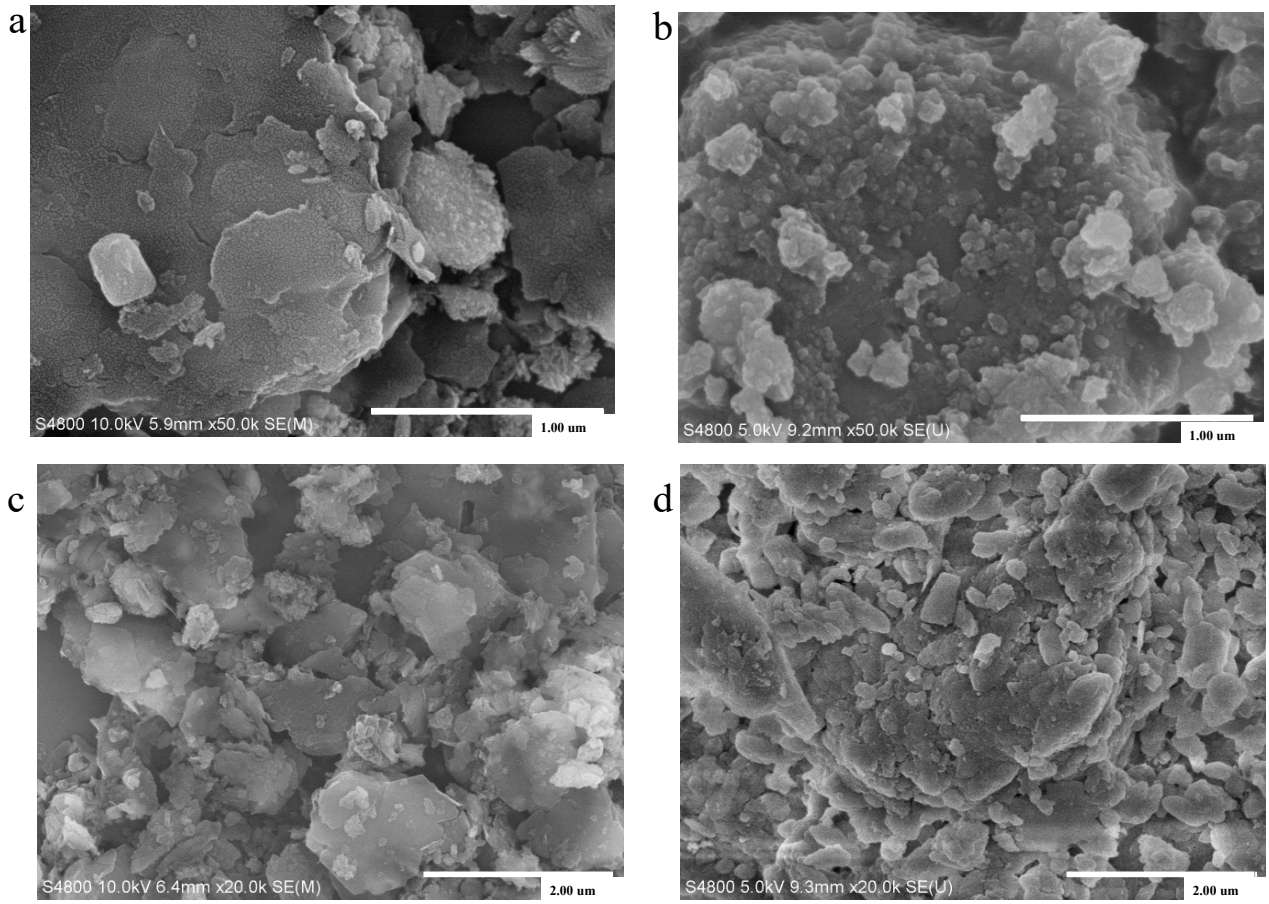

Figure 9. SEM images of HCG before (**a**) and after adsorption (**b**–**d**) are the SEM of KCG before and after adsorption of U(VI).

3. Conclusions

We successfully synthesized cost-effective adsorbents, namely HCG and KCG, from CCG by a simple chemical modification. Besides the optimized porosity and surface area, the kalsilite formation in KCG conspicuously enhanced the affinity towards U(VI). As we showed here, KCG exhibited an excellent adsorption capacity (140 mg/g) under pH 6 within 120 min. The pseudo second-order model of the kinetic study indicated a chemical interaction dominated process. Making use of the solid waste, the elimination of radioactivity U(VI) was realized by a waste control by waste strategy. As most of the research is still in the early stage, obtaining an in-depth understanding of the controlled synthesis of kalsilite from minerals and the reusability of natural adsorbents remains ongoing.

Supplementary Materials: The following are available online at https://www.mdpi.com/article/10.3390/su13158421/s1, Figure S1: The XPS of CCG (black), HCG (red) and KCG (green), showing the characteristic peaks, Figure S2: The TGA (Line) and DSC (dots) of CCG (black), HCG (red) and KCG (green), Figure S3: The N2 adsorption isotherms at 77K (Left) and the pore size distributions using BHJ analysis (Right). CCG (black), HCG (red) and KCG (green), Figure S4: Effects of adsorption contact time on the removal efficiency of U(VI) onto HCG (black) and KCG (red), Figure S5: The isotherm linear plots of CCG (a), HCG(b), and KCG(c), Table S1: Adsorption capacity under variant pH condition (from 2 to 6) (mg/g).

Author Contributions: Data curation, Z.D.; Funding acquisition, M.L.; R.J. and J.Z.; Investigation, Y.G. and J.H.; Methodology, Y.G.; Resources, J.Z.; Supervision, R.J. All authors have read and agreed to the published version of the manuscript.

Funding: This research was funded by the National Science Fund for Distinguished Young Scholars (No. 51725403), the National Natural Science Foundation of China (No. 52004271), and Hunan Provincial Natural Science Foundation for Excellent Young Scholars (No. 2020JJ3028).

Institutional Review Board Statement: Not applicable.

Informed Consent Statement: Not applicable.

Data Availability Statement: All data generated or analysed during this study are included in this published article.

Acknowledgments: This work is supported by the National Science Fund for Distinguished Young Scholars (No. 51725403), the National Natural Science Foundation of China (No. 52004271), and Hunan Provincial Natural Science Foundation for Excellent Young Scholars (No. 2020JJ3028). The "Qihang Plan" fund of the China University of Mining and Technology is acknowledged.

Conflicts of Interest: The authors declare no conflict of interest.

References

1. Burnham, A.; Han, J.; Clark, C.E.; Wang, M.; Dunn, J.B.; Palou-Rivera, I. Life-Cycle Greenhouse Gas Emissions of Shale Gas, Natural Gas, Coal, and Petroleum. *Environ. Sci. Technol.* **2011**, *46*, 619–627. [CrossRef]
2. Huang, J.; Shiva Kumar, G.; Ren, J.; Sun, Y.; Li, Y.; Wang, C. Towards the potential usage of eggshell powder as bio-modifier for asphalt binder and mixture: Workability and mechanical properties. *Int. J. Pavement Eng.* **2021**, 1–13. [CrossRef]
3. Akcil, A.; Koldas, S. Acid Mine Drainage (AMD): Causes, treatment and case studies. *J. Clean. Prod.* **2006**, *14*, 1139–1145. [CrossRef]
4. Jabłońska, B.; Kityk, A.; Busch, M.; Huber, P. The structural and surface properties of natural and modified coal gangue. *J. Environ. Manag.* **2017**, *190*, 80–90. [CrossRef]
5. Huang, Y.; Zhang, J.; Yin, W.; Sun, Q. Analysis of overlying strata movement and behaviors in caving and solid backfill-ing mixed coal mining. *Energies* **2017**, *10*, 1057. [CrossRef]
6. Zhang, J.X.; Ju, Y.; Zhang, Q.; Ju, F.; Xiao, X.; Zhang, W.Q.; Li, M. Low ecological environment damage technology and method in coal mines. *J. Min. Strata Control Eng.* **2019**, *1*, 013515.
7. Li, J.; Wang, J. Comprehensive utilization and environmental risks of coal gangue: A review. *J. Clean. Prod.* **2019**, *239*, 117946. [CrossRef]
8. Huang, J.; Duan, T.; Zhang, Y.; Liu, J.; Zhang, J.; Lei, Y. Predicting the permeability of pervious concrete based on the beetle antennae search algorithm and random forest model. *Adv. Civ. Eng.* **2020**, *2020*, 8863181.
9. Huang, J.; Sun, Y.; Zhang, J. Reduction of computational error by optimizing svr kernel coefficients to simulate concrete compressive strength through the use of a human learning optimization algorithm. *Eng. Comput.* **2021**, 1–18. [CrossRef]

10. Karakosta, C.; Pappas, C.; Marinakis, V.; Psarras, J. Renewable energy and nuclear power towards sustainable develop-ment: Characteristics and prospects. *Renew. Sustain. Energy Rev.* **2013**, *22*, 187–197. [CrossRef]
11. García-Balboa, C.; Baselga-Cervera, B.; García-Sanchez, A.; Igual, J.M.; Lopez-Rodas, V.; Costas, E. Rapid adaptation of microalgae to bodies of water with extreme pollution from uranium mining: An explanation of how mesophilic organisms can rapidly colonise extremely toxic environments. *Aquat. Toxicol.* **2013**, *144–145*, 116–123. [CrossRef] [PubMed]
12. Duan, S.; Xu, X.; Liu, X.; Wang, Y.; Hayat, T.; Alsaedi, A.; Li, J. Highly enhanced adsorption performance of U (VI) by non-thermal plasma modified magnetic Fe_3O_4 nano-particles. *J. Colloid Interface Sci.* **2018**, *513*, 92–103. [CrossRef] [PubMed]
13. Huang, J.; Zhang, Y.; Sun, Y.; Ren, J.; Zhao, Z.; Zhang, J. Evaluation of pore size distribution and permeability reduction behavior in pervious concrete. *Constr. Build. Mater.* **2021**, *290*, 123228. [CrossRef]
14. Veliscek-Carolan, J. Separation of actinides from spent nuclear fuel: A review. *J. Hazard. Mater.* **2016**, *318*, 266–281. [CrossRef]
15. Abney, C.W.; Mayes, R.T.; Saito, T.; Dai, S. Materials for the Recovery of Uranium from Seawater. *Chem. Rev.* **2017**, *117*, 13935–14013. [CrossRef] [PubMed]
16. Vellingiri, K.; Kim, K.-H.; Pournara, A.; Deep, A. Towards high-efficiency sorptive capture of radionuclides in solution and gas. *Prog. Mater. Sci.* **2018**, *94*, 1–67. [CrossRef]
17. Wang, X.; Chen, L.; Wang, L.; Fan, Q.; Pan, D.; Li, J.; Wang, X. Synthesis of novel nanomaterials and their application in efficient removal of radionuclides. *Sci. China Chem.* **2019**, *62*, 933–967. [CrossRef]
18. Carboni, M.; Abney, C.; Liu, S.; Lin, W. Highly porous and stable metal–organic frameworks for uranium extraction. *Chem. Sci.* **2013**, *4*, 2396–2402. [CrossRef]
19. Nekhunguni, P.M.; Tavengwa, N.T.; Tutu, H. Sorption of uranium (VI) onto hydrous ferric oxide-modified zeolite: As-sessment of the effect of pH, contact time, temperature, selected cations and anions on sorbent interactions. *J. Environ. Manag.* **2017**, *204*, 571–582. [CrossRef] [PubMed]
20. Munir, M.A.M.; Liu, G.; Yousaf, B.; Mian, M.; Ali, M.U.; Ahmed, R.; Cheema, A.I.; Naushad, M. Contrasting effects of biochar and hydrothermally treated coal gangue on leachability, bioavailability, speciation and accumulation of heavy metals by rapeseed in copper mine tailings. *Ecotoxicol. Environ. Saf.* **2020**, *191*, 110244. [CrossRef]
21. Mohammadi, R.; Azadmehr, A.; Maghsoudi, A. Fabrication of the alginate-combusted coal gangue composite for simul-taneous and effective adsorption of Zn(II) and Mn(II). *J. Environ. Chem. Eng.* **2019**, *7*, 103494. [CrossRef]
22. Li, D.; Song, X.; Gong, C.; Pan, Z. Research on cementitious behavior and mechanism of pozzolanic cement with coal gangue. *Cem. Concr. Res.* **2006**, *36*, 1752–1759. [CrossRef]
23. Moghadam, M.J.; Ajalloeian, R.; Hajiannia, A. Preparation and application of alkali-activated materials based on waste glass and coal gangue: A review. *Constr. Build. Mater.* **2019**, *221*, 84–98. [CrossRef]
24. Selvam, T.; Inayat, A.; Schwieger, W. Reactivity and applications of layered silicates and layered double hydroxides. *Dalton Trans.* **2014**, *43*, 10365–10387. [CrossRef]
25. Jabłońska, B.; Siedlecka, E. Removing heavy metals from wastewaters with use of shales accompanying the coal beds. *J. Environ. Manag.* **2015**, *155*, 58–66. [CrossRef]
26. Zhou, L.; Zhou, H.; Hu, Y.; Yan, S.; Yang, J. Adsorption removal of cationic dyes from aqueous solutions using ceramic adsorbents prepared from industrial waste coal gangue. *J. Environ. Manag.* **2019**, *234*, 245–252. [CrossRef] [PubMed]
27. Li, H.; Zheng, F.; Wang, J.; Zhou, J.; Huang, X.; Chen, L.; Liu, J.L. Facile preparation of zeolite-activated carbon composite from coal gangue with enhanced adsorption perfor-mance. *Chem. Eng. J.* **2020**, *390*, 124513. [CrossRef]
28. Qiu, R.; Cheng, F.; Huang, H. Removal of Cd2+ from aqueous solution using hydrothermally modified circulating fluid-ized bed fly ash resulting from coal gangue power plant. *J. Clean. Prod.* **2018**, *172*, 1918–1927. [CrossRef]
29. Yan, S.; Pan, Y.; Wang, L.; Liu, J.; Zhang, Z.; Huo, W.; Yang, J.; Huang, Y. Synthesis of low-cost porous ceramic microspheres from waste gangue for dye adsorption. *J. Adv. Ceram.* **2017**, *7*, 30–40. [CrossRef]
30. Zhao, H.; Huang, X.; Liu, F.; Hu, X.; Zhao, X.; Wang, L.; Gao, P.; Li, J.; Ji, P. Potential of a novel modified gangue amendment to reduce cadmium uptake in lettuce (Lactuca sativa L.). *J. Hazard. Mater.* **2021**, *410*, 124543. [CrossRef] [PubMed]
31. Meng, F.; Yu, J.; Tahmasebi, A.; Han, Y. Pyrolysis and combustion behavior of coal gangue in O_2/CO_2 and O_2/N_2 mixtures using thermogravimetric analysis and a drop tube furnace. *Energy Fuels* **2013**, *27*, 2923–2932. [CrossRef]
32. Zhou, J.; Zheng, F.; Li, H.; Wang, J.; Bu, N.; Hu, P.; Gao, J.-M.; Zhen, Q.; Bashir, S.; Liu, J.L. Optimization of post-treatment variables to produce hierarchical porous zeolites from coal gangue to enhance adsorption performance. *Chem. Eng. J.* **2020**, *381*, 122698. [CrossRef]
33. Becerro, A.I.; Escudero, A.; Mantovani, M. The hydrothermal conversion of kaolinite to kalsilite: Influence of time, temperature, and pH. *Am. Miner.* **2009**, *94*, 1672–1678. [CrossRef]
34. Purbasari, A.; Samadhi, T.W.; Bindar, Y. Thermal and Ash Characterization of Indonesian Bamboo and Its Potential for Solid Fuel and Waste Valorization. *Int. J. Renew. Energy Dev.* **2016**, *5*, 95–100. [CrossRef]
35. Novembre, D.; Gimeno, D.; D'Alessandro, N.; Tonucci, L. Hydrothermal synthesis and characterization of kalsilite by using a kaolinitic rock from Sardinia, Italy, and its application in the production of biodiesel. *Mineral. Mag.* **2018**, *82*, 961–973. [CrossRef]
36. Novembre, D.; Gimeno, D. The Solid-state Conversion of Kaolin to Kalsio4 Minerals: The Effects of Time and Temperature. *Clays Clay Miner.* **2017**, *65*, 355–366. [CrossRef]
37. Su, S.-Q.; Ma, H.-W.; Yang, J.; Zhang, P.; Luo, Z. Synthesis of kalsilite from microcline powder by an alkali-hydrothermal process. *Int. J. Miner. Met. Mater.* **2014**, *21*, 826–831. [CrossRef]

38. Zhang, N.; Ejtemaei, M.; Nguyen, A.V.; Zhou, C. XPS analysis of the surface chemistry of sulfuric acid-treated kaolinite and diaspore minerals with flotation reagents. *Miner. Eng.* **2019**, *136*, 1–7. [CrossRef]
39. Guo, Y.; Yan, K.; Cui, L.; Cheng, F. Improved extraction of alumina from coal gangue by surface mechanically grinding modification. *Powder Technol.* **2016**, *302*, 33–41. [CrossRef]
40. Shao, D.; Hou, G.; Li, J.; Wen, T.; Ren, X.; Wang, X. PANI/GO as a super adsorbent for the selective adsorption of uranium(VI). *Chem. Eng. J.* **2014**, *255*, 604–612. [CrossRef]